Engineering with Computers (2022) 38 (Suppl 1):S607–S628
https://doi.org/10.1007/s00366-020-01165-x

ORIGINAL ARTICLE

Combination of baffling technique and high-thermal conductivity fluids to enhance the overall performances of solar channels

Younes Menni[1] · Mahyar Ghazvini[2] · Houari Ameur[3] · Myeongsub Kim[2] · Mohammad Hossein Ahmadi[4] · Mohsen Sharifpur[5,6]

Received: 12 June 2020 / Accepted: 31 August 2020 / Published online: 15 September 2020

Abstract

In the present study, two-phase flow and forced-convection heat transfer of hydrogen gas (H_2) in a solar finned and baffled channel heat exchanger (SFBCHE) is studied numerically. The effect of different obstacles in the channel is addressed. A H_2 heat transfer fluid (HTF) having a high thermal conductivity with the baffling technique is implemented to enhance the overall performance of a solar channel. In the initial step, the results from the proposed numerical model were compared with the experimental data of a smooth channel, and then against data with a baffled channel. After checking the validity of our model, the same numerical approach was used for studying thermal-fluid characteristics of the channel with the new fluid. A hydrothermal analysis is presented for a range of Reynolds number (Re) from 5000 to 25,000. At the lowest Re = 5000, the thermal enhancement factor (TEF) is about 1.25. This value increases to 2.16, or 73.46%, when Re = 10,000. This increase in the TEF values continues as Re increases. The largest Re = 25,000 gives the highest TEF value, as it is about 4.18, which is 2.75 times greater than that given for the case of using the conventional gaseous fluid (air). Therefore, our proposed structure for the SFBCHE with high H_2 HTF flow velocity leads to improve the values of dynamic pressure (P_d) and heat transfer (Nu), while reducing the skin friction (f) values, which increases the overall TEF of the channel. In addition, all performance values are greater than unity (or 1.00). This reflects the importance of the H_2 HTF baffling and finning technique in improving the hydrodynamic thermal-energy performance of solar heat exchangers. The suggested model of SFBCHE filled with an H_2 HTF having a high thermal conductivity allows a considerable enhancement in the overall thermal performances which can be employed in various thermal types of equipment, such as solar energy receivers, automotive radiators, and cooling in chemical industries.

Keywords Computational fluid dynamics · Hydrogen working fluid · Finning technology · Numerical analysis · Solar heat exchanger · Solar receivers

List of symbols

c_1	Constant in k–ε model
c_2	Constant in k–ε model
Cf	Local coefficient of friction
Cp	Specific heat, J kg^{-1} K^{-1}
D_h	Hydraulic diameter, m
f	Average coefficient of friction
f_0	Friction Factor for smooth exchanger
H	Height of exchanger, m
h	Height of detached baffle, m

✉ Mahyar Ghazvini
mghazvini2020@fau.edu

✉ Mohsen Sharifpur
mohsensharifpur@duytan.edu.vn;
mohsen.sharifpur@up.ac.za

[1] Unit of Research on Materials and Renewable Energies, Department of Physics, Faculty of Sciences, Abou Bekr Belkaid University, P.O. Box 119, 13000 Tlemcen, Algeria

[2] Department of Ocean and Mechanical Engineering, Florida Atlantic University, 777 Glades Road, Boca Raton, FL 33431, USA

[3] Department of Technology, University Centre of Naama (Ctr Univ Naama), PO Box 66, 45000 Naama, Algeria

[4] Faculty of Mechanical Engineering, Shahrood University of Technology, Shahrood, Iran

[5] Institute of Research and Development, Duy Tan University, Da Nang 550000, Vietnam

[6] Department of Mechanical and Aeronautical Engineering, University of Pretoria, Pretoria 0002, South Africa

h'	Height of attached fin, m
k	Kinetic energy of turbulence, $m^2\ s^{-2}$
L	Length of exchanger, m
L_{ex}	Fin-exit space, m
L_{in}	Inlet-baffle space, m
Nu	Average Nusselt number
Nu_0	Nusselt number for smooth exchanger
Nu_x	Local Nusselt number
P	Pressure, Pa
Pd	Dynamic pressure, Pa
Pr	Prandtl number
Re	Reynolds number
S	Fin-baffle space, m
T	Temperature, K
TEF	Thermal performance
u	X-velocity, m s^{-1}
U_{in}	Intake velocity, m s^{-1}
u_m	Mean velocity of the section, m s^{-1}
v	Y-velocity, m s^{-1}
W	Channel width, m
ΔP	Pressure drop, Pa

Greek letters

Γ	Coefficient of turbulent diffusion
ε	Rate of dissipation, $m^2\ s^{-3}$
λ	Thermal conductivity, W $m^{-1}\ K^{-1}$
μ	Dynamic viscosity, kg $m^{-1}\ s^{-1}$
μ_e	Effective viscosity, kg $m^{-1}\ s^{-1}$
μ_l	Laminar viscosity, kg $m^{-1}\ s^{-1}$
μ_t	Turbulent viscosity, kg $m^{-1}\ s^{-1}$
ρ	Density, kg m^{-3}
σ_k	Constant in k-equation
σ_ε	Constant in ε-equation
σ_T	Constant in energy equation
τ_w	Wall shear stress, Pa

Subscript

0	Smooth
e	Effective
ex	Exit
f	Fluid
in	Intake
l	Laminar
s	Solid
t	Turbulent
w	Wall
x	Local

1 Introduction

Solar heat exchangers are thermal devices that are used in solar systems to convert solar radiation into heat energy [1, 2]. They typically consist of multiple channels at millimeter to centimeter scales. Due to the increasing demand for the use of thermal energy, research on advanced channel designs has become prominent to achieve high energy efficiency by improving their flow and thermal characteristics [3–7]. In particular, the main focus of numerous studies is on improving the flow and thermal behaviors inside the solar channels when the channel has extended areas with baffles and fins [8–12]. The baffling method is considered as one of the most extensively applied approaches in enhancing thermal performance of various industrial systems like solar collectors, internal cooling thermal regenerators, shell-and-tube heat exchangers (STHEs), electronic cooling devices, and static mixers [13–16]. Introduction of baffles, fins, and ribs disturbs the fluid flow over the entire channel with the creation of reverse currents, leading to a good mixing of the fluid and intensified turbulence of the fluid flow, as a result, enhances thermal transfer [17, 18]. Generally, these baffles, fins, and ribs, which increase turbulence flow are considered as turbulators. Various shapes of turbulators have been used in different experimental and numerical investigations to enhance the thermal performance of solar collectors.

Using experimental methods, Liu et al. [19] studied the characteristics of heat transfer over ribs inside steam-cooled rectangular channels for Re number from 10,000 to 80,000. In this study, the influencing parameters were Re number, channel aspect ratio, and channel blockage ratio. Based on their results, the average Nusselt number (Nu) for a channel with $\alpha = 60°$ is approximately 15–25% lower than that for $\alpha = 45°$. Ali et al. [20] experimentally showed the improvement of the steady forced-convection heat transfer over triangular-type cylinders. Four cylinders with different cross-section lengths were considered, and local and total Nusselt numbers were measured to determine temperature across the surface. Kumar et al. [21] experimentally used discrete W-shaped ribs to increase heat transfer inside roughened ducts. The effects of attachment angle, Re numbers, relative roughness, and pitch on friction and heat transfer have been investigated. They found that, Nu number was enhanced and the friction factor was reduced by increasing Re numbers. Additionally, using both solid and perforated baffles, Karwa et al. [22] enhanced hydrothermal performances of rectangular ducts for a range of Re numbers 2850–11,500. According to the results, Nu number for the solid baffles increased 73.7–82.7% compared with the smooth duct. Kabeel et al. [23] examined the influence of longitudinal fin heights on the solar baffled collector characteristics with different airflow rates. The fins' heights used in this study were 3, 5, and 8 cm. They concluded that the modified entrance resulted in enhancing efficiency and output temperature.

Also, Cao et al. [24] performed experimental and numerical analyses to improve the thermal performance of the heat exchanger using sextant helical baffles in a STHE. It was reported that while the heat transfer coefficient and pressure

drop reduced at a specific mass flow rate, the heat transfer coefficient per unit pressure drop augmented. Saedodin et al. [25] carried out experimental and numerical studies to determine the thermal enhancement of a flat-plate solar collector in the presence of a porous metal material. Their results show that the Nusselt number and thermal efficiency were increased up to 82% and 18.5%, respectively, compared with a collector without porous materials. Abchouyeh et al. [26] carried out a numerical analysis using Lattice Boltzmann method to determine the thermal performance of a sinusoidal-baffled horizontal channel filled with water/Cu nanofluid. They reported that the mean values of Nu number were increased with the increase in the nanoparticle fraction and the decrease in the obstacle space. Using both wedge-type ribs and winglet geometry vortices generators, Chompookham et al. [27] worked on the enhancement of convective heat transfer of air inside a channel in turbulent flow. To make the flow turbulent, two kinds of right-triangle ribs have been proposed. Based on the results, significant heat transfer enhancement and pressure drop were achieved using the wedge ribs. Dutta and Hossain [28] experimentally augmented the characteristics of local heat transfer as well as the skin friction through a rectangular channel by using inclined solid and perforated baffles with a Re number from 12,000 to 41,000. In this experiment, two baffles with identical size were inserted in the channel. According to the results, the orientation, position and geometry of the second baffle are significantly affected by the local Nusselt number. Kalaiarasi et al. [29] showed energy and exergy analyses of a flat-plate solar air heater. This heater was made of copper with copper fins on both sides. It was concluded that the maximum exergy and energy efficiencies were 18.25–37.53% and 49.4–59.2, respectively. Peng et al. [30] showed a new type of air solar collectors using pin–fin on its absorber to enhance thermal efficiency. Based on the experimental results, the heat transfer coefficients of finned collectors are three times higher than flat-plate collector at air volume flow rate of 19 $m^3\ h^{-1}$.

In addition to experimental approaches, Selimefendigil et al. [31] performed a finite element method-based numerical study of hydrothermal characteristics of convective laminar Fe_3O_4–water nanofluid through a bifurcating-type channel with a variable magnetic field. The authors showed an enhanced heat transfer by about 9–12% as well as 12–15% on the presence and absence of a magnetic field, respectively. Chamkha et al. [32] and Menni et al. [33] performed numerical study to determine forced-convective heat transfer in a channel equipped with fins and baffles with air flow. Izadi et al. [34] used nanofluid including carbon nanotubes in a 3D rectangular channel exposed to opposed buoyant forces to measure convection heat transfer. They found that the heat transfer rate reduces with an increase in the opposed buoyancy. A CFD simulation of a solar air heat channel has been performed by Menni et al. [35] to determine heat transfer enhancement using complicated geometry fins. According to the results, higher heat transfer enhancement was observed using arc-fins at Re = 12,000. In another study, Menni et al. [35] analyzed convective heat transfer in a channel with diamond-shaped baffles in turbulent flow with Re numbers between 12,000 and 32,000. Based on the results, heat transfer and skin friction improvements were 3.962–29.82 times higher than channel without baffles, respectively.

Using numerical techniques, Kamali and Binesh [36] investigated the turbulent heat transfer and analyzed the characteristics of friction through a square duct with different ribs such as trapezoidal, triangular, and square shapes. According to the results, the rip shape has a significant effect on the convective heat transfer coefficient. Also, higher thermal improvement can be achieved using trapezoidal ribs. Using Robin boundary conditions, Umavathi and Sheremet [37] employed Runge–Kutta shooting scheme to investigate the impact of both electric and magnetic fields on the mixed convective heat transfer flow inside a vertical section channel with a heat source/sink. Their results were presented in terms of an average speed and Nusselt number.

Nasiruddin and Siddiqui [38] enhanced the heat transfer inside a circular tube by inserting a baffle. The influence of baffle orientation and size on the thermal performance of the channel was studied. It was concluded that a significant enhancement in the Nu number was obtained by increasing the baffle height for a vertical baffle. On the other hand, the pressure loss was considerable. Wang et al. [39] improved the heat transfer in a rectangular channel by installing pin fins. Various shapes of pin fins were used in this study such as drop shaped, elliptical, and circular. It was reported that the circular-shaped pin fins have a higher heat transfer enhancement compared with drop-shaped fins (approximately 26% difference in the average Nu number). Using a numerical scheme, Eiamsa-ard and Promvonge [40] reported the characteristics of the forced-convection heat transfer in the presence of transverse grooves on the bottom surface of a 2D channel. The variable parameters used in the study were Re number between 6000 and 18,000 and width to channel height ratio from 0.5 to 1.75. As reported in the results, 158% heat transfer improvement was obtained using the grooved channel when compared with the smooth channel. Employing circular-type rings, Ozceyhan et al. [41] simulated the heat transfer and friction loss in a tube using circular cross-sectional rings with different spacings. The simulation was performed with FLUENT with Re number from 4475 to 43,725. As reported in the results, reducing ring spacing leads to an increase in the Nu number and friction factor. Furthermore, Promvonge et al. [42] simulated a 3D structure of the turbulent regime flow and thermal transfer inside a square channel containing '*V*' discrete-type ribs. Finite volume method with SIMPLE algorithm was

used in this simulation. It was reported that the heat transfer in the channel equipped with ribs is 200–370% greater than the smooth channel without ribs. Sripattanapipat and Promvonge [43] numerically studied the effects of inserting diamond-shaped baffles with various tip angles on the thermal enhancement in a 2D channel. It was reported that the baffle angle reduction resulted in a rise in the friction factor and Nu number. Using Lattice Boltzmann method, Pirouz et al. [44] simulated the conjugate heat transfer inside a rectangular channel with attached obstacles. This study was performed under the condition of different Re numbers, distance between obstacles, and thermal diffusivity. Based on the results, convective heat transfer rate is increased by reducing the distance between obstacles which leads to the flow deviation. Mohammadi and Sabzpooshani [45] performed an energy analysis and simulated the improvement of heat transfer inside a baffled solar heater under external recycle effect. This recycle effect was provided by using a recycle device attached at the end of the upper channel. It was concluded that using fins with external recycle is a suitable method to increase energy efficiency. Mohammadi et al. [46] studied the enhancement of heat transfer in a solar heater with fins and baffles in terms of outlet air temperature and effective efficiency. According to the results, using this technique leads to an increase in the outlet air temperature compared with a simple channel. Using both numerical and experimental techniques, Skullong et al. [47] investigated the enhancement of heat transfer inside a square duct fitted by oblique horseshoe baffles. The studied parameters included different relative baffle pitches and heights, and Re numbers. Priyam and Chand [48] studied the impact of flow rate on the solar collector efficiency in the case of air heat transfer flow and an absorber mounted with wavy fins. They also presented the impact of the deflector number on its heat transfer behavior. Additionally, Hu et al. [49] numerically investigated a solar air collector with baffles to evaluate heat transfer characteristics and internal flow. The effects of air gap thickness, baffle number, and operating conditions on the performance of the collector were studied. Bayrak et al. [50] studied energy and exergy analyses of a solar air heater by inserting porous baffles with different thicknesses. The used porous materials were closed-cell aluminum foams with 6-mm and 10-mm thickness. According to the results, the greatest efficiency and air temperature can be obtained by a solar air heater with the 6-mm baffle. Youcef-Ali and Desmons [51] reported, through experimental and numerical analysis, the efficiency of a solar collector with fins on its flat plate absorber. More numerical studies of convective laminar and turbulent flows in baffled and finned heat exchanger channels can be found in the literature (Dadvand et al. [52], Luo et al. [53], Muñoz-Cámara et al. [54], Mellal et al. [55], Miroshnichenko et al. [56], Promvonge et al. [57], Wang et al. [39], Wen et al. [58], Yongsiri et al. [59], Mokhtari et al. [60], Arjmandi et al. [61], and Wang et al. [62]) as reported in Table 1.

As indicated earlier, many investigators have focused their analyses on how to enhance the flow through the channel heat exchangers contained in these solar energy collectors, such as adding extended surfaces with baffles, fins and ribs. In most of these studies, the only fluid considered is air. Air has inefficient thermo-physical properties, such as density and thermal conductivity. For this reason, the thermal performance of these thermal collectors is less effective in industrial applications. This paper combines two different approaches and evaluates the effectiveness of this strategy on the heat transfer enhancement. The 1st approach is to divert the fluid flow by inserting vortex generators and, therefore, creating gaps, secreting vortices and allowing the fluid to acquire important thermal energy. The 2nd approach is to compensate the air with a high-thermal conductivity (λ_f) fluid like hydrogen fluid to augment the heat transfer between the two areas (hot wall and working fluid). In this study, the hydrothermal behavior of the adopted hydrogen fluid is analyzed by investigating flow fields. The flow is evaluated in terms of dynamic pressure, stream function, average, axial and transverse velocities, turbulent kinetic energy, turbulent intensity, turbulent viscosity, and temperature, as well as analyzing dimensionless axial velocity and dynamic pressure curves at different locations of the channel to reveal the fluid flow field characteristics of each region. The characteristics of heat transfer, friction, and performance factor are also presented.

2 Mathematical modeling

2.1 Computational domain

In the present study, two-phase flow and heat transfer of hydrogen gas (H_2) in a channel with different obstacles is studied. Schematic of the computational domain with different obstacles is addressed as reported in Fig. 1. This study is of practical interest due to a systematical analysis of the effect of a detached baffle and attached flat fins.

The implementation of a H_2 HTF having a high λ_f with the baffling technique will guarantee the enhancement of the overall thermal performance of the heat exchanger channel.

The geometrical dimensions used in this study, i.e., L, L_{in}, L_{ex}, D_h, S, H, h and w, are those reported by Demartini et al. [63] in their numerical and experimental study of a heat exchanger containing vertical plates attached to both horizontal walls of the fluid stream (Table 2).

In this study, a combination analysis of two technologies is addressed. The 1st technology is to divert the stream by including turbulators (a detached baffle plate and an attached fin pair) and, therefore, creating gaps,

Table 1 Representative studies of finned and baffled channels for enhancing heat transfer

Investigators	Method - Software	Simulated domain flow field
Dadvand et al. [52]	Finite Element Method Commercial COMSOL Multiphysics version 5.4	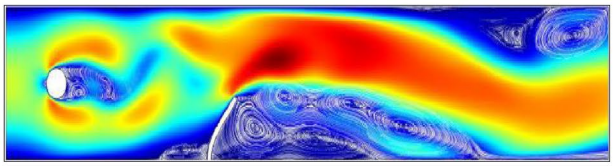
Luo et al. [53]	Finite Volume Method Commercial ANSYS CFX	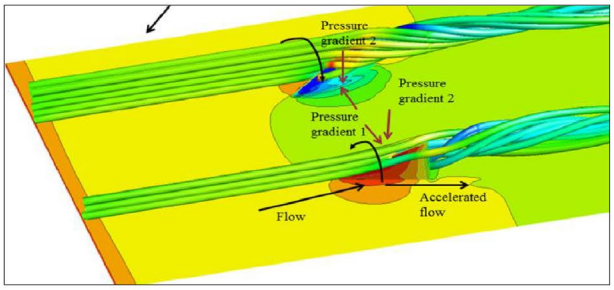
Muñoz-Cámara et al. [54]	Finite Volume Method ANSYS Fluent 18	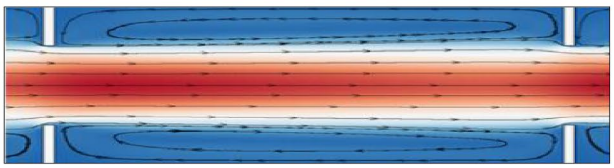
Mellal et al. [55]	Finite Element Method CFD COMSOL Multiphysics 5.1	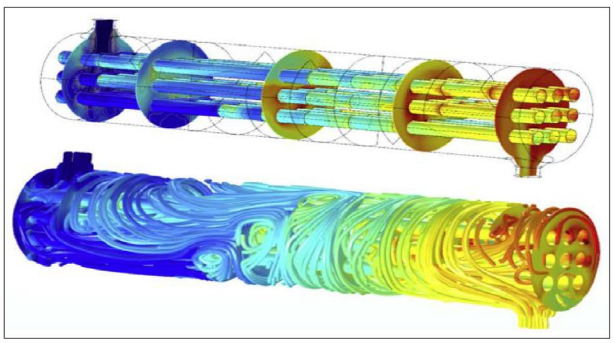
Miroshnichenko et al. [56]	Finite Difference Method	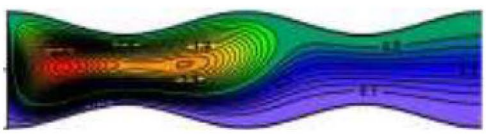
Promvonge et al. [57]	Finite Volume Method CFD Fluent	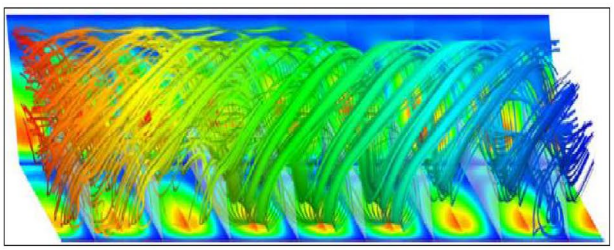

Table 1 (continued)

Wang et al. [39]	Finite Volume Method CFD Fluent	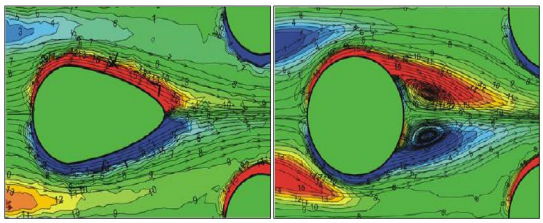
Wen et al. [58]	Finite Volume Method ANSYS Fluent 15	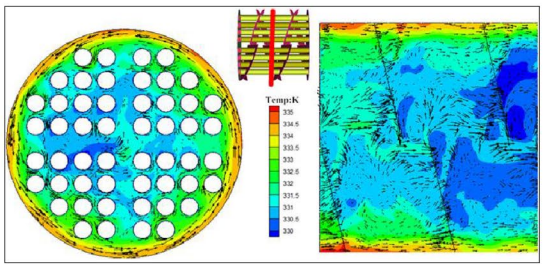
Yongsiri et al. [59]	Finite Volume Method CFD Fluent	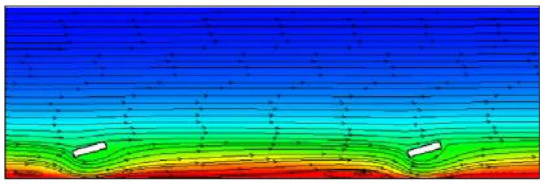
Mokhtari et al. [60]	Finite Volume Method CFD Fluent	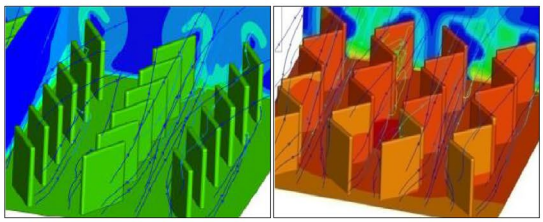
Arjmandi et al. [61]	Finite Volume Method ANSYS Fluent 19	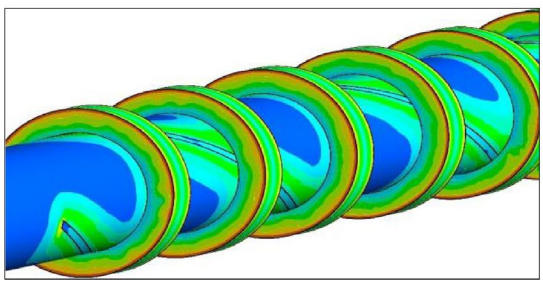
Wang et al. [62]	Finite Volume Method CFD Fluent 16.0	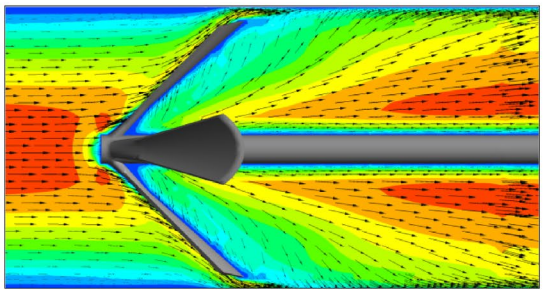

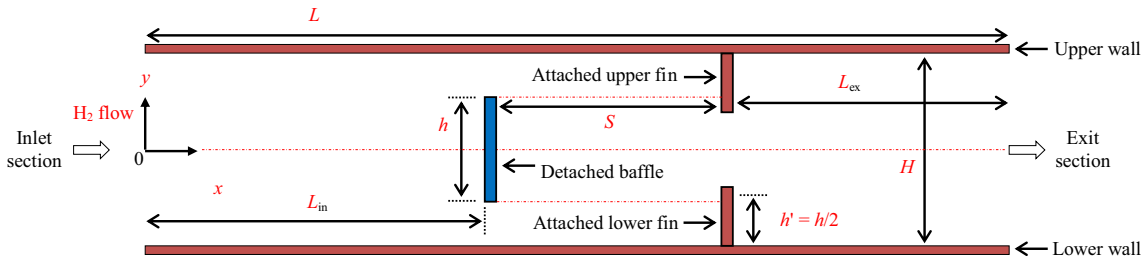

Fig. 1 Schematic of a computational domain. Specific dimensions of the geometry and properties of fluid and solid walls are shown in Tables 2, 3, 4

Table 2 Geometrical dimensions of the present baffled and finned channel [63]

Dimension	Value (m)
Channel length (L)	0.554
Inlet–baffle distance (L_{in})	0.218
Baffle–fin separation distance (S)	0.142
Fins-exit distance (L_{ex})	0.174
Channel height (H)	0.146
Channel hydraulic diameter (D_h)	0.167
Baffle height (h)	0.08
Baffle and fin width (w)	0.01

Table 3 Thermal and physical properties of H_2 HTF [64]

Name	Material type
Hydrogen	Fluid
Chemical formula	Fluent fluid materials
H_2	Hydrogen (H_2)
Properties	Values
Density, ρ_f (kg m^{-3})	0.08189
Specific heat at constant pressure, Cp_f (J kg^{-1} K^{-1})	14283
Thermal conductivity, λ_f (W m^{-1} K^{-1})	0.1672
Viscosity, μ_f (kg m^{-1} s^{-1})	8.41×10^{-6}

Table 4 Thermal and physical properties of aluminum (Al) solid wall [64]

Name	Material type
Aluminum	Solid
Chemical formula	Fluent fluid materials
Al	Aluminum (Al)
Properties	Values
Density, ρ_s (kg m^{-3})	2719
Specific heat at constant pressure, Cp_s (J kg^{-1} K^{-1})	871
Thermal conductivity, λ_s (W m^{-1} K^{-1})	202.4

secreting vortices and allowing the fluid to acquire important thermal energy. The 2nd technology is to compensate the air with a high-λ_f fluid like H_2 fluid to raise the transport of heat between the two hot wall and working fluid sections.

The thermal and physical properties of the used H_2 HTF and aluminum (Al) solid wall are shown in Tables 3 and 4, respectively. On the other hand, the performance of the traditional gaseous fluid, which is air (its thermal conductivity of 0.0242 W m^{-1} K^{-1} thermal conductivity), is presented to compare and highlight the effectiveness of the new hydrogen-based fluid in promoting heat transfer.

2.2 Physical model

Several assumptions are considered in this analysis:

- H_2 HTF flow is steady,
- H_2 HTF flow is turbulent,
- H_2 HTF is incompressible (Mach number is less than 0.3; its value is about 0.002 at the smallest Re value, while it is about 0.012 for the maximum value of the same variable).
- H_2 HTF density ρ_f is constant,
- H_2 HTF specific heat Cp_f is constant,
- H_2 HTF dynamic viscosity μ_f is constant,
- H_2 HTF thermal conductivity λ_f is constant, and
- Al solid thermal physical properties are constant.

2.3 Governing equations

The governing equation describing the fluid flow within the baffled and finned heat exchanger channel can be written as follows [65]:

$$\frac{\partial}{\partial x}(\rho u\phi)+\frac{\partial}{\partial y}(\rho v\phi)=\frac{\partial}{\partial x}\left[\Gamma_\phi\frac{\partial\phi}{\partial x}\right]+\frac{\partial}{\partial y}\left[\Gamma_\phi\frac{\partial\phi}{\partial y}\right]+S_\phi, \tag{1}$$

with

- $\phi \equiv (u, v, k, \varepsilon \text{ and } T)$,
- u: x-velocity,
- v: y-velocity,
- k: turbulent kinetic energy,
- ε: turbulent dissipation rate,
- Γ_ϕ: turbulent diffusion coefficient, and
- S_ϕ: source term.

Equations for ϕ, Γ_ϕ and S_ϕ [65]:
Continuity:

$$\phi = 1, \tag{2}$$

$$\Gamma_\phi = 0, \tag{3}$$

$$S_\phi = 0. \tag{4}$$

X-momentum:

$$\phi = u, \tag{5}$$

$$\Gamma_\phi = \mu_e, \tag{6}$$

$$S_\phi = -\frac{\partial p}{\partial x}. \tag{7}$$

Y-momentum:

$$\phi = v, \tag{8}$$

$$\Gamma_\phi = \mu_e, \tag{9}$$

$$S_\phi = -\frac{\partial p}{\partial y}. \tag{10}$$

Fluid energy:

$$\phi = T, \tag{11}$$

$$\Gamma_\phi = \frac{\mu_e}{\sigma_T}, \tag{12}$$

$$S_\phi = 0. \tag{13}$$

Turb-kinetic energy (k):

$$\phi = k, \tag{14}$$

$$\Gamma_\phi = \mu_l + \frac{\mu_l}{\sigma_k}, \tag{15}$$

$$S_\phi = -\rho.\varepsilon + G. \tag{16}$$

Turbulence dissipation rate (ε):

$$\phi = \varepsilon, \tag{17}$$

$$\Gamma_\phi = \mu_l + \frac{\mu_t}{\sigma_\varepsilon}, \tag{18}$$

$$S = \frac{\varepsilon}{k}(c_1 G - c_2 \rho \varepsilon), \tag{19}$$

with

$$\mu_e = \mu_l + \mu_t, \tag{20}$$

$$G = \mu_t \left\{ 2.\left(\frac{\partial u}{\partial x}\right)^2 + 2.\left(\frac{\partial v}{\partial y}\right)^2 + \left(\frac{\partial v}{\partial x} + \frac{\partial u}{\partial y}\right)^2 \right\}, \tag{21}$$

where

- c_1, c_2, σ_k, σ_ε and σ_T: turbulent constants for standard k–ε model.
- μ_e: the effective viscosity.
- μ_t: turbulent viscosity.
- μ_l: laminar viscosity.

2.4 Boundary conditions

The detached baffled and attached finned heat exchanger channel is simulated according to the following hydrothermal boundary conditions:

- H_2 HTF, at $T_{in} = 300$ K, flows into the channel,
- A uniform, one-dimensional velocity field ($u = U_{in}$ at $x = 0$) is considered at the inlet, and atmospheric pressure ($P = P_{atm}$ at $x = L$) at the exit,
- The top and bottom channel walls, as well as the fin attachment surfaces, are kept at constant temperature ($T_w = 375$ K at $y = \pm H/2$), and
- Impermeable boundary and no-slip wall conditions are applied for the solid walls.

The equations to satisfy these boundary conditions are given below:

- At the inlet section ($x = 0$, $-H/2 \le y \le H/2$),

$$u = U_{in} \tag{22}$$

$$v = 0 \tag{23}$$

$$T = T_{in} = 300 \text{ K} \tag{24}$$

$$k = k_{\text{in}} = 0.005U_{\text{in}}^2 \tag{25}$$

$$\varepsilon = \varepsilon_{\text{in}} = 0.1k_{\text{in}}^2. \tag{26}$$

- At the channel walls (top wall at $0 \le x \le L$, $y = H/2$, and bottom wall at $0 \le x \le L$, $y = -H/2$),

$$u = v = 0 \tag{27}$$

$$k = \varepsilon = 0 \tag{28}$$

$$T = T_{\text{w}}. \tag{29}$$

- At the outlet section ($x = L$, $-H/2 \le y \le H/2$),

$$P = P_{\text{atm}} \tag{30}$$

$$\frac{\partial \phi}{\partial x} = 0. \tag{31}$$

2.5 Governing parameters

- Channel hydraulic diameter (D_{h}),

$$D_{\text{h}} = \frac{2HW}{(H+W)}. \tag{32}$$

- Reynolds number (Re),

$$\text{Re} = \frac{\rho u_{\text{m}} D_{\text{h}}}{\mu}. \tag{33}$$

- Skin friction coefficient (*Cf*),

$$\text{Cf} = \frac{2\tau_{\text{w}}}{\rho u_{\text{m}}^2}. \tag{34}$$

- Friction factor (*f*),

$$f = \frac{2(\Delta P/L)D_{\text{h}}}{\rho u_{\text{m}}^2}. \tag{35}$$

- Local Nusselt number (Nu_x),

$$\text{Nu} = \frac{h(x)D_{\text{h}}}{\lambda_{\text{f}}}. \tag{36}$$

- Average Nusselt number (Nu),

$$\text{Nu} = \frac{1}{L}\int \text{Nu}_x \partial x. \tag{37}$$

- Correlation of Dittus and Boelter [66],

$$\text{Nu}_0 = 0.023\text{Re}^{0.8}\,\text{Pr}^{0.4}. \tag{38}$$

- Correlation of Petukhov [67],

$$f_0 = (0.79Ln\text{Re} - 1.64)^{-2} \quad \text{for } 3000 \le \text{Re} \le 5 \times 10^6. \tag{39}$$

3 Numerical modeling

3.1 Numerical model

A two-dimensional domain of a solar baffled and finned heat exchanger channel filled with H_2 HTF is considered. This domain was meshed by employing structured-type, quadrilateral-shape, non-uniform grids. The H_2 HTF flow is in turbulence, and standard *k*–epsilon (ε) model [68] with finite volume method (FVM) [69] is utilized to study the model. The near-wall treatment function, discretization schemes, iterative scheme, flow field prediction algorithm, under-relaxation factors as well as the convergence criteria are shown in detail in Table 5.

3.2 Grid independence

To avoid the effect of grid density ($n_x \times n_y$) on the numerical solution, we changed the number of mesh nodes from 95 to 345 according to the horizontal axis ($y = 0$), while from 35 to 145 according to the vertical axis ($x = 0$). The effect of varying node density values on H_2 HTF flow filed characteristics in terms of maximum dimensionless axial velocity ($u_{\text{max}}/U_{\text{in}}$) and maximum dynamic pressure (Pd_{max}) is shown in Table 6, for $\text{Re} = 5 \times 10^3$.

Depending on the obtained thermodynamic and thermal values, it was found that the relative errors, Er and Er′, calculated by Eqs. (40) and (41), for changing the values of $u_{\text{max}}/U_{\text{in}}$ and Pd_{max} do not exceed, respectively 0.148 and 0.182%, when the node density changes from (245 × 95) to (370 × 145).

$$\text{Er} = \frac{(u_{\text{max}}/U_{\text{in}})_{\text{ref}} - u_{\text{max}}/U_{\text{in}}}{(u_{\text{max}}/U_{\text{in}})_{\text{ref}}} \times 100, \tag{40}$$

$$\text{Er} = \frac{(\text{Pd}_{\text{max}})_{\text{ref}} - \text{Pd}_{\text{max}}}{(\text{Pd}_{\text{max}})_{\text{ref}}} \times 100. \tag{41}$$

This indicates that there is no benefit of increasing the mesh values from (245 × 95) to (370 × 145) cells. Therefore, the density of the grid of (245 × 95) cells is taken for optimum numerical achievement.

Table 5 Solution controls

Governing equations		Discretization schemes	
Continuity		Pressure	Second Order
Momentum		Momentum	QUICK
Turbulent kinetic energy		Turbulent kinetic energy	QUICK
Turbulent dissipation rate		Turbulent dissipation rate	QUICK
Energy		Energy	QUICK
Near-wall treatment function		**Pressure-velocity coupling algorithm**	
Standard wall functions		SIMPLE	
Under-relaxation factors		**Iterative scheme**	
Pressure	0.3	Implicit	
Density	1	**Convergence criteria**	
Body forces	1	Continuity	10^{-6}
Momentum	0.7	x-velocity	10^{-6}
Turbulent kinetic energy	0.8	y-velocity	10^{-6}
Turbulent dissipation rate	0.8	Turbulent kinetic energy	10^{-6}
Turbulent viscosity	1	Turbulent dissipation rate	10^{-6}
Energy	1	Energy	10^{-9}

Table 6 Variation of u_{max}/U_{in} and Pd_{max} with $(n_x \times n_y)$ node density, $Re = 5 \times 10^3$

$(n_x \times n_y)$	(95×35)	(120×45)	(145×55)	(170×65)	(195×75)	(220×85)	(245×95)	(370×145)
u_{max}/U_{in}	3.140	3.180	3.217	3.291	3.345	3.351	3.353	3.358
Er (%)	6.491	5.300	4.198	1.995	0.387	0.208	0.148	Reference
Pd_{max}	4.090	4.142	4.190	4.287	4.357	4.365	4.368	4.376
Er′ (%)	6.535	5.347	4.250	2.033	0.434	0.251	0.182	Reference

3.3 Verification of a smooth rectangular channel

The heat transfer (Nu_0) curves, as well as the data of friction coefficients (f_0), are shown in Fig. 2a, b, respectively, for a rectangular channel, with smooth walls, crossed by a hydrogen (H_2 HTF) stream. Both the numerical values of (Nu_0) and (f_0) were compared with the experimental values obtained by the two empirical correlations of Dittus and Boelter [66], and Petukhov [67], respectively. From the figures, at variable Re values from 5×10^3 to 2.5×10^4, it is clear that there is a quantitative convergence between the numerical and experimental solutions, in terms of Nu_0 and f_0. This indicates the validity of the numerical methodology used in this simulation for smooth channels with no obstacles.

3.4 Validation of a baffled and finned rectangular channel

There is also a comparison of the numerical and experimental data from the literature, but only concerns are about the case of the baffled channel heat exchanger. The comparison is made in terms of the pressure coefficient curves. This comparison is performed using the same engineering structure, similar fluid flow conditions, and numerical and experimental analysis performed by Demartini et al. [63] and his researchers in their referenced paper.

They used air as a working fluid within the conduit of a shell-and-tube heat exchanger channel [63]. As shown in Fig. 3, the pressure coefficient values were compared in two different cross-positions, respectively $x = 0.345$ m and $x = 0.405$ m, for a constant value of Reynolds number of 8.73×10^4, i.e., $U_{in} = 7.8$ m/s. The results of the comparison show adequate coordination between the CFD values of our simulations and the numerical and experimental values reported by Demartini et al. [63], under the same conditions of the experiment. Based on this, we consider that the numerical model used is valid, and we employed the same numerical method for hydrogen gas (H_2 HTF).

4 Results and discussion

The originality of the present work is the implementation of a H_2 HTF having a high thermal conductivity with the baffling technique to enhance the overall performance of the heat exchanger. Therefore, our results are compared

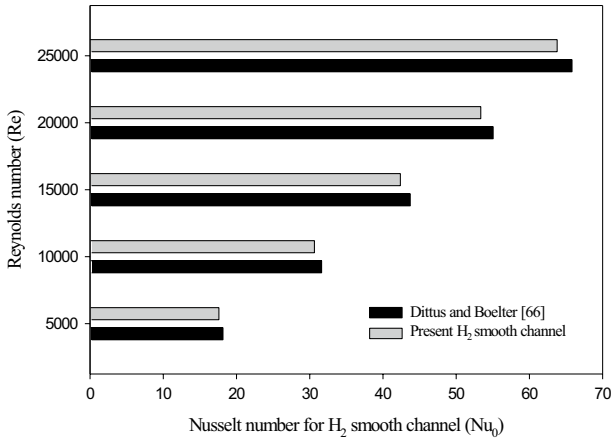

(a) Profiles of Nusselt number of smooth channel (Nu_0) compared with Dittus and Boelter [66]

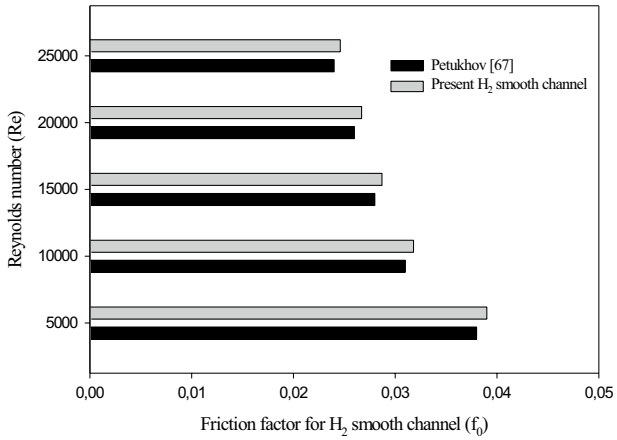

(b) Profiles of friction factor of smooth channel (f_0) compared with Petukhov [67]

Fig. 2 Verification of heat transfer and friction loss for smooth rectangular channel with H_2 HTF

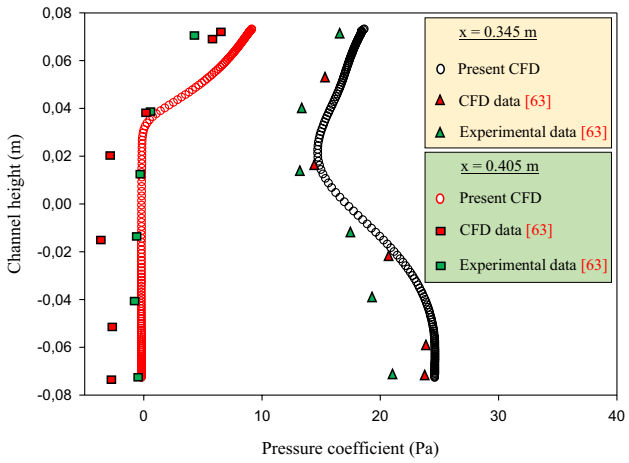

Fig. 3 Control of fluid flow field, in terms of pressure coefficient, by comparing it with the numerical and experimental data of Demartini et al. [63], using similar experience conditions, i.e., 2D channel, two baffle plates, air fluid, and $U_{in} = 7.8$ m/s

against an experimental data of a H_2 smooth channel heat exchanger, and then against a baffled channel. So, the identical approach has been applied for the new fluid after checking the validity of our numerical model.

From Fig. 4, it is clear that the dynamic pressure (Pd) values are high next to the top (see zone 'A' in Figs. 4, 5a) and bottom (see zone 'B' in Figs. 4, 5a) edges of the baffle, while they are low on its left and right sides. The dynamic pressure values are also high in areas located between the backside of the baffle and the front sides of the fins, next to the duct walls.

The Pd values are very high between the two upper edges of the fins, across the gap (see zone 'C' in Figs. 4, 5b) up to the duct outlet. As expected, the Pd values increase across the gaps (see zones 'A', 'B', and 'C' in Figs. 4, 5) as a result of the decrease in the flow area due to the presence of obstacles. In addition, the dynamic pressure value is important at the high values of Re number.

Streamlines are normal from the inlet of the channel, while they are disturbed as the flow approaches the obstacles, as shown in Fig. 6. The H_2 current flows at high dynamic pressure through the gaps while creating very strong cells for recycling due to the decrease in dynamic pressure values on the rear sides of the obstacles (see zones 'D', 'E', and 'F'. As expected, the height, length and strength of recycling cells increase with increasing Re number values, as shown in Fig. 7a, b.

The mean velocity (V) values are very low on the back of the obstacles due to the presence of recycling cells (see Fig. 8). The mean speed values increase in areas adjacent to the upper and lower edges of the baffle as a result of high dynamic pressure in these regions, while they are very high across the gap formed between the edges of the fins.

As is clear, there is a large area, located between the top and bottom recycling cells, extending from the edges of the fins to the duct outlet, with very high flow mean speeds, due to the presence of the single outlet, under high dynamic pressure across the last gap. As expected, there is a direct

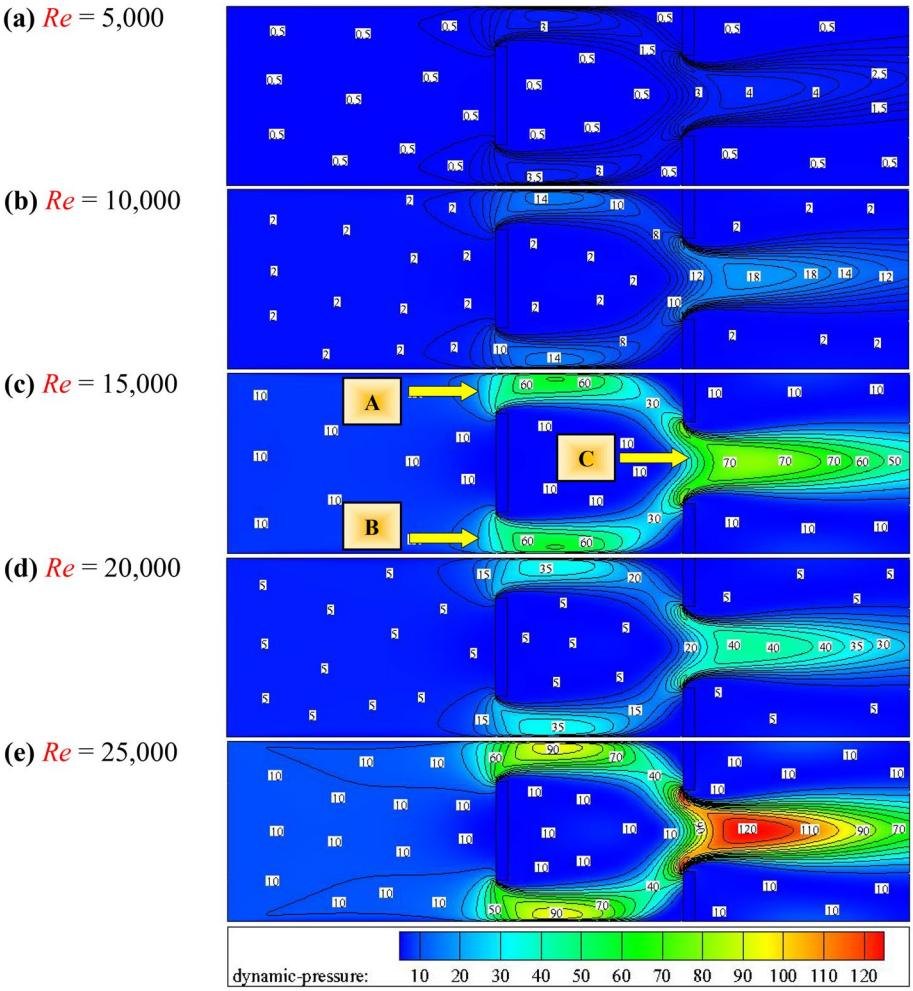

Fig. 4 Variation of Pd (in Pa) with Re

correlation between mean speed values and Re number values, as shown in Fig. 9.

It is clear that the axial velocity (u or x-speed) values are very low on the rear sides of all obstacles due to the presence of recycling cells (see zones 'D', 'E', and 'F' in Fig. 10). These cells are reverse flows with negative velocities. Conversely, the axial velocity values are very high across the gaps, especially at large Reynolds values.

The y-velocity (v or y-speed) values are very high on the upper front edge of the baffle, while they are very low on their lower front edge, as shown in Fig. 11a. Also, the y-velocity values are very low on the upper front edge of the upper fin, while they are very high on the upper front edge of the bottom fin. Also, in Fig. 11a, the transverse velocity values improve in both direct and opposite directions with Reynolds number values.

In Fig. 11b, the turbulence intensity (TI) is low next to the left and right sides of the obstacles while increased next to the upper and lower edges of the baffle as well as through the last gap between the upper edges of the fins, for a wide range of Reynolds numbers. As expected, the intensity of the turbulence is important for the high values of Reynolds number.

The turbulent kinetic energy (k) values are very high at the center of the last gap, while they are medium, away from the back sides of the fins to the duct exit, as shown in Fig. 11c. However, the k values are low on the rest areas of the duct. As reported in this same figure, the higher the Reynolds number, the higher the kinetic energy, especially between the upper edges of the fins.

The H_2 fluid temperature values are high in areas adjacent to the sides of the fins, especially on its rear sides

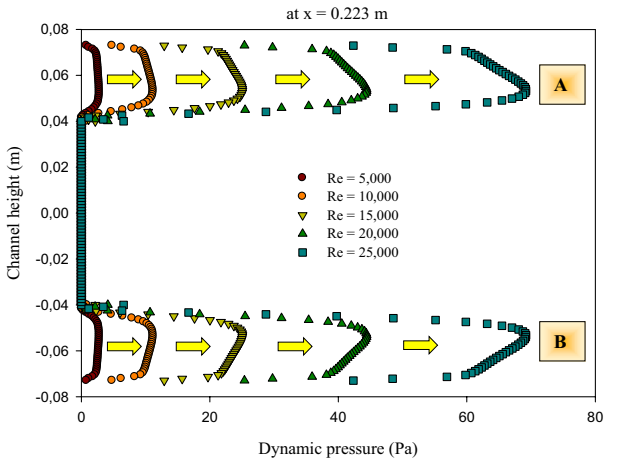

(a) at $x = 0.223$ m

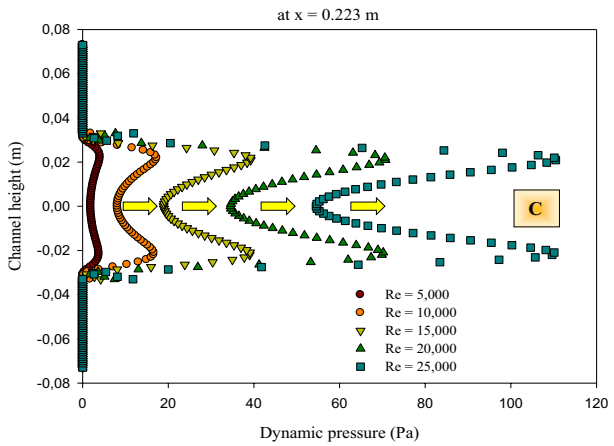

(b) at $x = 0.375$ m

Fig. 5 Profiles of Pd for various Re values

where the recycling cells are located, near the top and bottom duct surfaces, while they are very low across the three gaps, as shown in Fig. 11d. The temperature values are inversely proportional to the Reynolds number. The high thermal gradients are found near the upper and lower edges of the baffle, as well as on the upper edges of the fins, especially in the case of large Reynolds numbers, while they are low next to the bases of the fins and on their back region. The thermal gradient is directly proportional to the velocity and dynamic pressure values as well as the Reynolds number.

Figure 12 shows the profiles of local Nu_x/Nu_0 ratios for the top duct surface (at $y = H/2$) in the case of $Re = 5000$. The Nu_x/Nu_0 values are important in the vicinity of the top rear edge of the baffle plate. This area has high-temperature gradients, as a result of the current passing through the upper gap under the high pressure and high speed. In the rear region of the same baffle plate, Nu_x/Nu_0 values are high due to the presence of a strong flow recirculation on the right side. These values are reduced as the H_2 HTF approaches the top fin. This fin directs the H_2 HTF towards the lower duct section, and therefore, a contact reduction between the H_2 gas fluid and the top duct surface.

The values of local Nu_x/Nu_0 ratios are increased after the fin obstacle because of the presence of a large recirculation cell next to the duct top wall. Thus, the presence of obstacles in the field of H_2 flow leads to the good mixing of the fluid by generating large cells for recycling on the backsides. Also, the presence of obstacles allows the current to pass through narrow spaces under the high dynamic pressure and high speed with high-temperature gradients and, thus, increased heat transfer. The Nu_x/Nu_0 values are greatly improved if Re values increase. The analysis of Nu_x/Nu_0 results also shows a direct dependency on Re values, as shown in Fig. 13a.

Figure 13b shows the Re effects on the mean Nu/Nu_0 ratio for the top duct surface. It is clear that the Nu/Nu_0 values are greater than 1 in all cases of Re numbers. This means that heat transfer of the duct with obstacles is better than that of the smooth duct. In addition, Nu/Nu_0 values are greatly dependent on the Reynolds number, especially for large Re numbers. As it can be observed, the variation of normalized average Nusselt number is considerable by increasing the Re number. This is a confirmation of the previous figure (see Fig. 13a).

Figure 14 shows the normalized local skin friction coefficient (Cf/f_0) profiles for the top duct surface at a fixed $Re = 5000$. It is clear that the Cf/f_0 values are high in the rear areas of the obstacles where the recycling cells are located. The Cf/f_0 values are low next to the left part of the top fin obstacle due to the deviation of the H_2 current towards the last gap between the upper edges of the fins. The Cf/f_0 values are also neglected on the front part of the plate because the current is split into two streams towards the two holes adjacent to the edges of this baffle. As shown in this figure, the friction coefficients are maximum on the right of the upper edge of the baffle, due to the extreme deviation of the

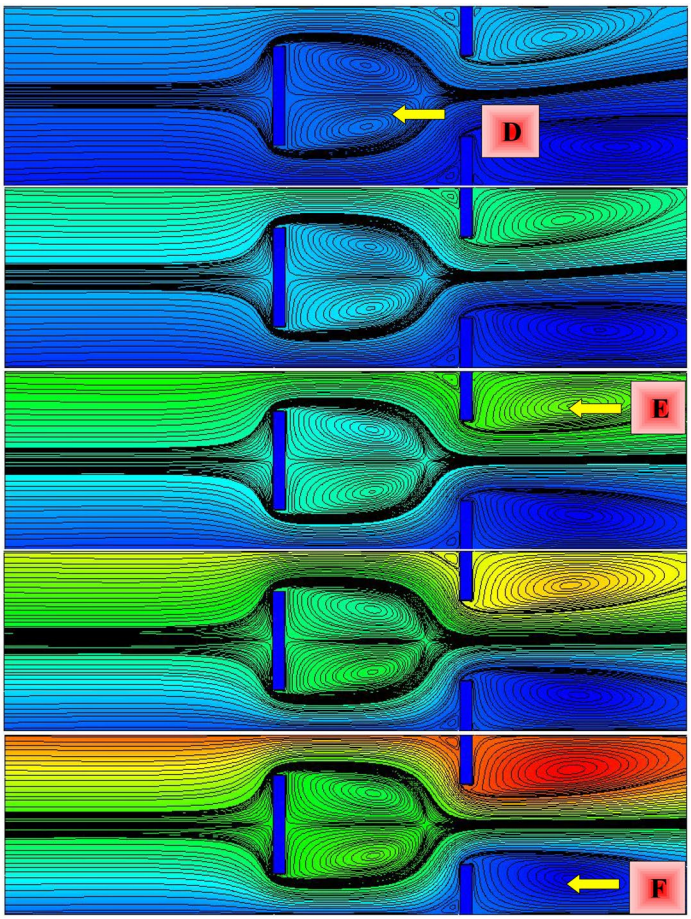

Fig. 6 Streamlines for different Re values

current across the upper gap under high dynamic pressure and high speed.

The effect of variations of Reynolds numbers on the local friction coefficients (Cf/f_0) is also studied, as shown in Fig. 15a. In the range of Re = 5000–25,000, the velocity values increase considerably, due to the significant increase in the dynamic pressure across the gaps, which reduces friction values. That is, this decrease in the friction values, recorded for the large values of Reynolds number, is due to the rapid flow of fluid current, and its traversal of contact areas at very high speed, which does not allow the fluid to come into contact with the entire channel wall.

The Reynolds number effects on the mean f/f_0 ratio for the top channel surface are also studied as shown in Fig. 15b. From this figure, the f/f_0 values exceed 1 in all cases of Reynolds numbers. This shows an increase in the skin friction in the channel with obstacles when compared to that in the smooth channel. This augmentation enhances as the Re number decreases.

Thermal performance factor (TEF) curves are included for Reynolds numbers from 5000 to 25,000 to highlight the importance of the hydrogen fluid used with the technique of deflectors (obstacles) in improving the overall thermal performance of the channel as depicted in Fig. 16. This parameter is calculated using the following relationship:

$$\mathrm{TEF} = \left(\mathrm{Nu}/\mathrm{Nu}_0\right)/\left(f/f_0\right)^{1/3}. \tag{47}$$

At the lowest Re = 5000, the performance factor is about 1.25. This value increases to 2.16, or 73.46%, when the Re = 10,000. This improvement in the *TEF* values continues as the Re number increases. As can be seen, the

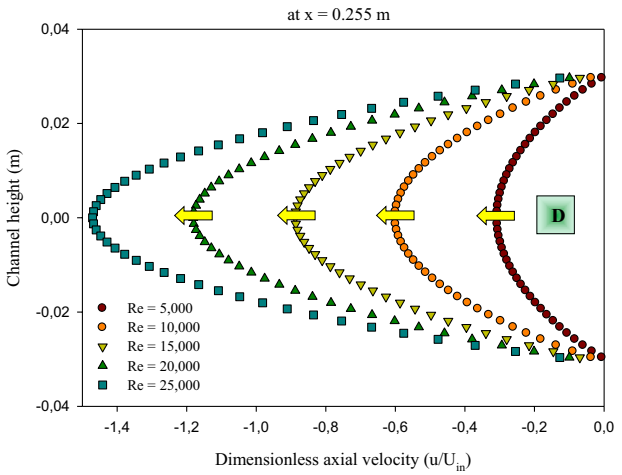

(a) Downstream of the detached baffle at x = 0.255 m

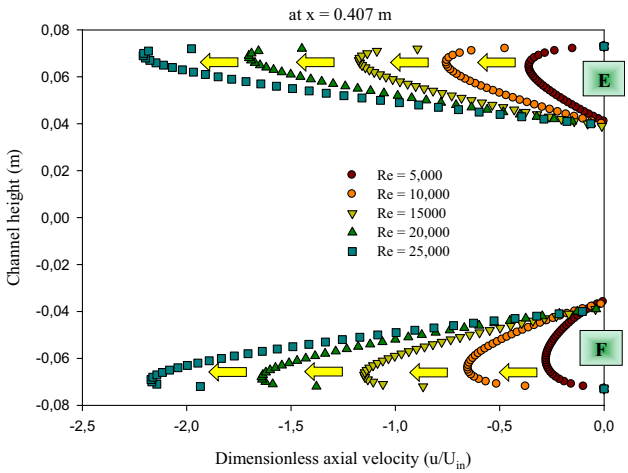

(b) Behind the attached fins at x = 0.407 m

Fig. 7 Effect of Re number on the length of recycling cells

largest Re = 25,000 gives the highest TEF value, as it is about 4.18, which is 2.75 times greater than that given for the case of using the conventional gaseous fluid (air). Therefore, designing the proposed SFBCHE with high H_2 fluid flow velocity has a significant effect on the thermal performance of the channel. As an illustration, raising the value of the Reynolds number allows improving the values of dynamic pressure (Pd) and heat transfer (Nu), while reducing the skin friction (f) values, which increases the thermal enhancement factor (TEF) of the channel. In addition, all performance values are greater than unity (or 1.00). This reflects the importance of the H_2 HTF baffling and finning technique in improving the hydrodynamic thermal-energy performance of smooth channels.

5 Conclusion

The present work implements a H_2 HTF having a high thermal conductivity with the baffling technique to enhance the overall performance of a solar heat exchanger channel. We compare the results against experimental data of a smooth channel, and then against data with a baffled channel. After checking the validity of our numerical model, the same numerical scheme was used for the new fluid. The results included the following:

- Streamlines are normal from the inlet of the channel, while they are disturbed as the flow approaches the obstacles.
- The H_2 current flows at high dynamic pressure through the gaps while creating very strong cells for recycling, due to a decrease in dynamic pressure values, on the rear sides of the obstacles.
- The height, length and strength of recycling cells increase with increasing Reynolds numbers.
- The x-velocity values are very low on the rear sides of all obstacles due to the presence of recycling cells. These cells show reverse flows with negative velocities. Conversely, the axial velocity values are very high across the gaps, especially for large Reynolds numbers.
- The y-velocity values are very high on the upper front edge of the baffle, while they are very low on their lower front edge. Also, the y-velocity values are very low on the upper front edge of the upper fin while they are very high on the upper front edge of the bottom fin.

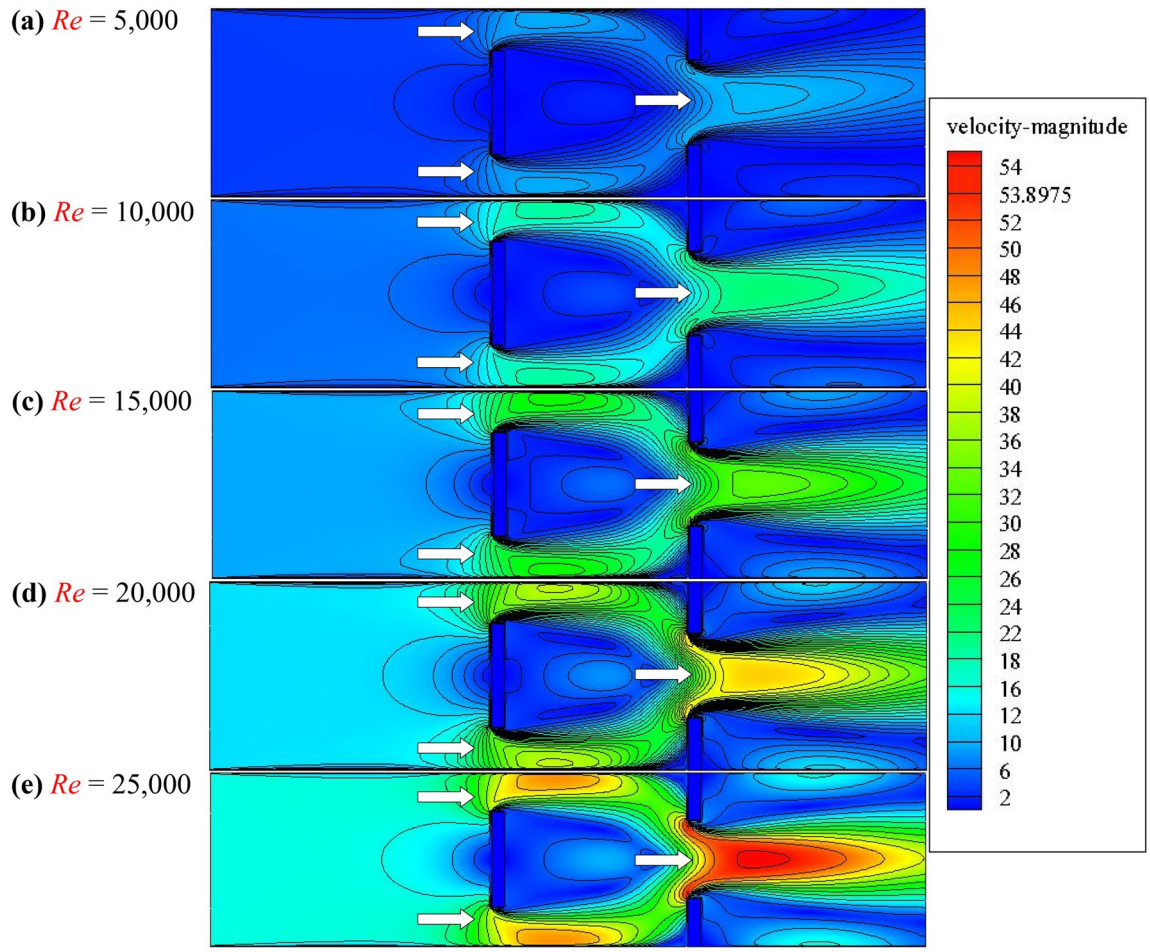

Fig. 8 Field of V (in m/s) for various Re values

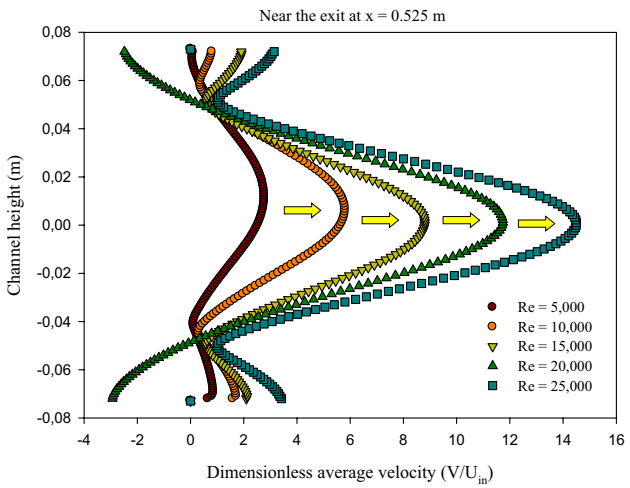

Fig. 9 Variation of dimensionless average velocity (V/U_{in}) with Re near the exit at $x = 0.525$ m

Also, the y-velocity values improve in both direct and opposite directions with Reynolds numbers.

- The turbulence intensity is low next to the left and right sides of the obstacles while increased next to the upper and lower edges of the baffle as well as through the last gap between the upper edges of the fins, for a wide range of Reynolds numbers. The intensity of the turbulence is extremely dependent on Re numbers, especially for the high values of Reynolds number.
- The Turb-kinetic-energy values are very high at the center of the last gap, while they are medium, away from the backside of the fins to the duct exit. The higher the Reynolds number, the higher the kinetic energy, especially between the upper edges of the fins.
- The H_2 fluid temperature values are high in areas adjacent to the sides of the fins, especially on its rear sides where the recycling cells are located, near the top and

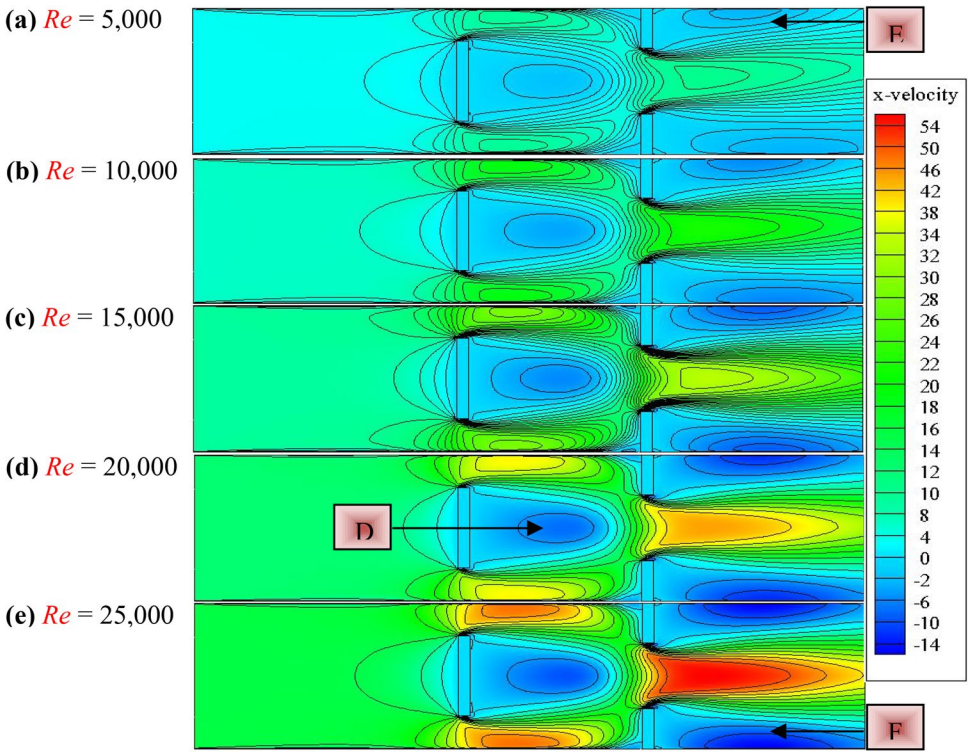

Fig. 10 Field of axial velocity (in m/s) for various Re values

bottom duct surfaces, while they are very low across the three gaps.

- The high thermal gradients are found near the upper and lower edges of the baffle, as well as on the upper edges of the fins, especially in the case of large Reynolds numbers, while they are low next to the bases of the fins and on their back region.
- The thermal gradient is directly proportional to the velocity and dynamic pressure values as well as the Reynolds number.
- For the lowest Re = 5000, the performance factor is about 1.25. This value increases to 2.16, or 73.46%, when the Re = 10,000. This increase in the *TEF* values continues as the Re number increases.
- The largest Reynolds number at 25,000, provides the highest thermal enhancement factor (TEF) value, which is about 4.18.
- Structuring the proposed baffled and finned heat exchanger channel with high H_2 fluid flow velocity, i.e. increasing the value of the Re number, allows to improve the values of dynamic pressure and heat transfer, while reducing the skin friction values, which increases the thermal enhancement factor (TEF) of the channel.
- All performance values are greater than unity (or 1.00). This reflects the importance of the H_2 HTF baffling and finning technique in improving the hydrodynamic thermal-energy performance of smooth channels.

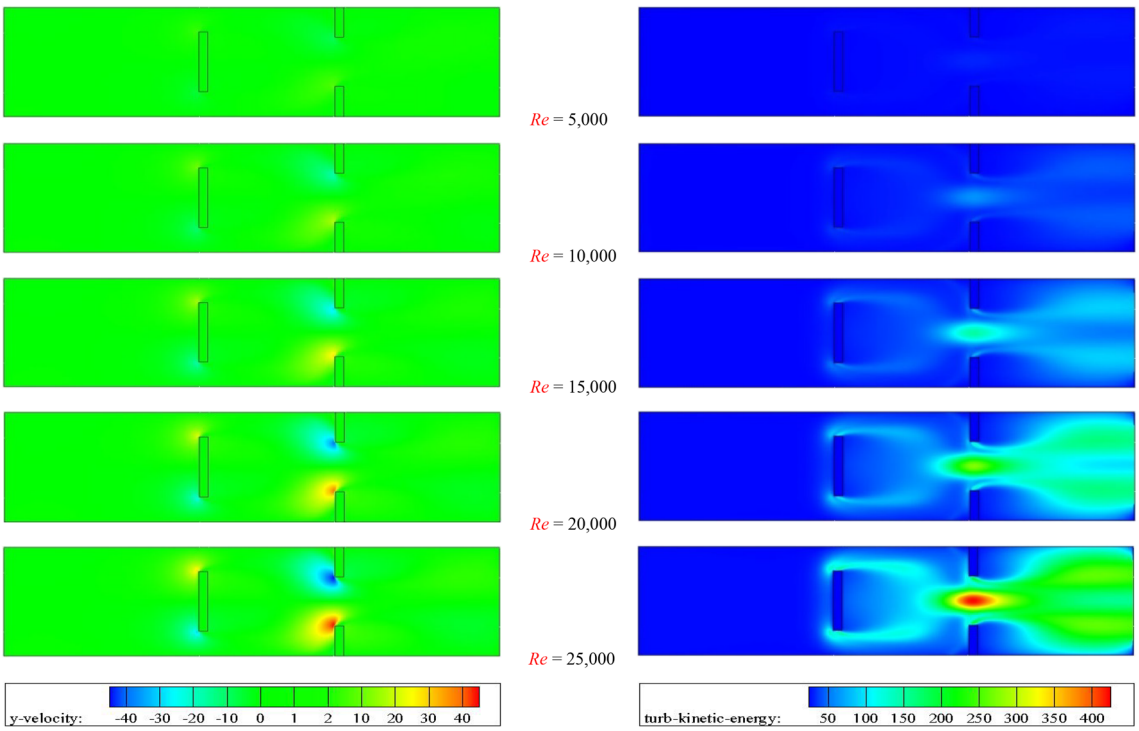

(a) Y-velocity (in m/s)

(c) Turb-kinetic-energy (in m^2/s^2)

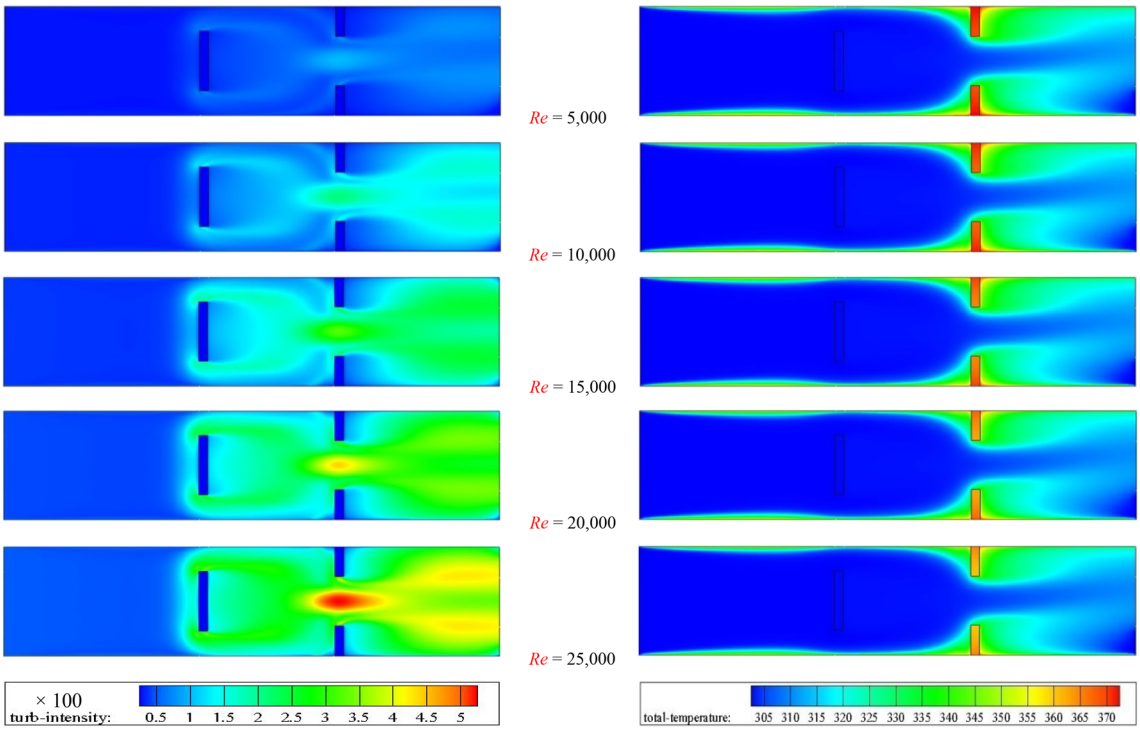

(b) Turb-intensity (in %)

(d) Temperature (in K)

Fig. 11 Other hydrothermal fields as a function of Re number

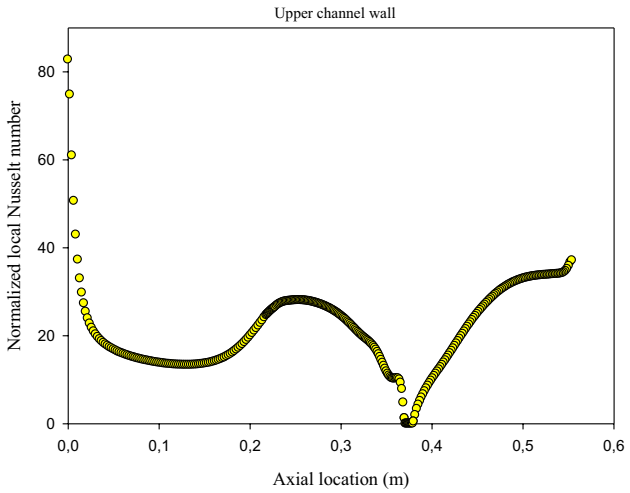

Fig. 12 Nu_x/Nu_0 profile for $y = H/2$ at Re = 5000

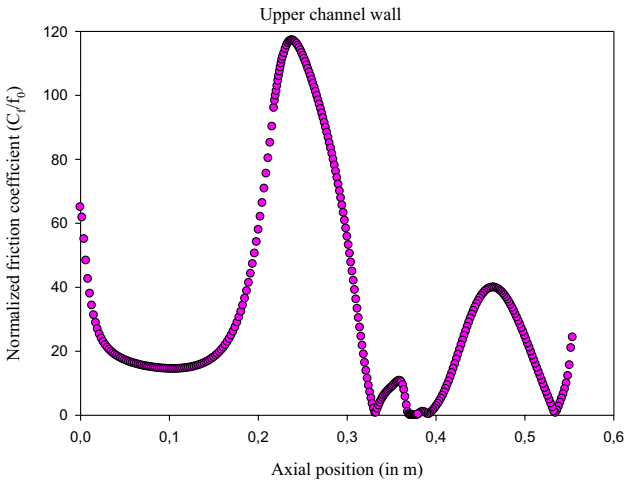

Fig. 14 Cf/f_0 profile for $y = H/2$ at Re = 5000

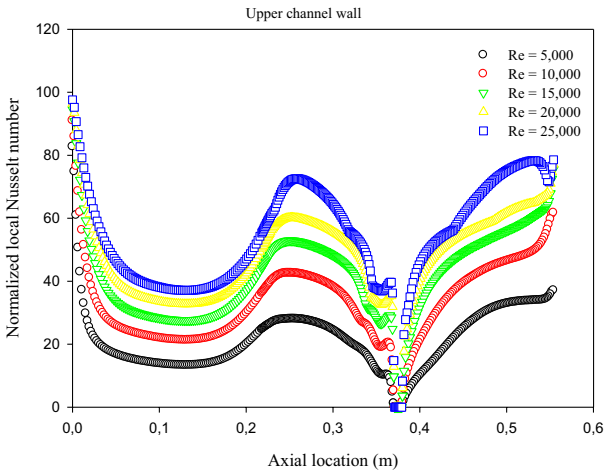

(a) Profiles of Nu_x/Nu_0

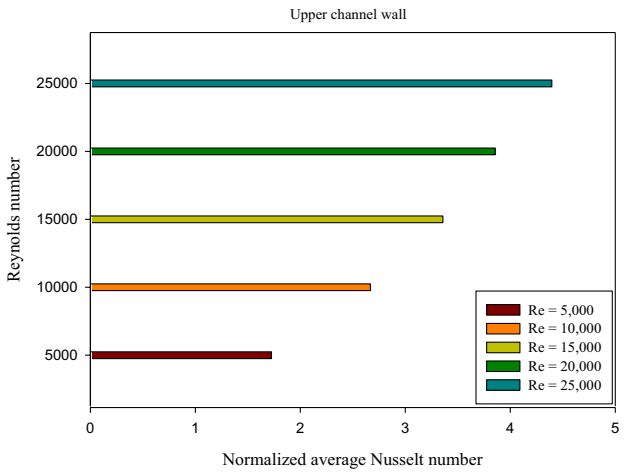

(b) Profiles of Nu/Nu_0

Fig. 13 Re effects on the local and average values of Nu at the top channel wall

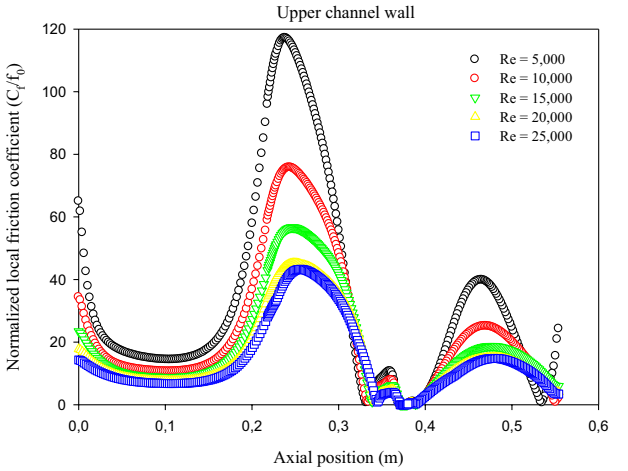

(a) Profiles of Cf/f_0

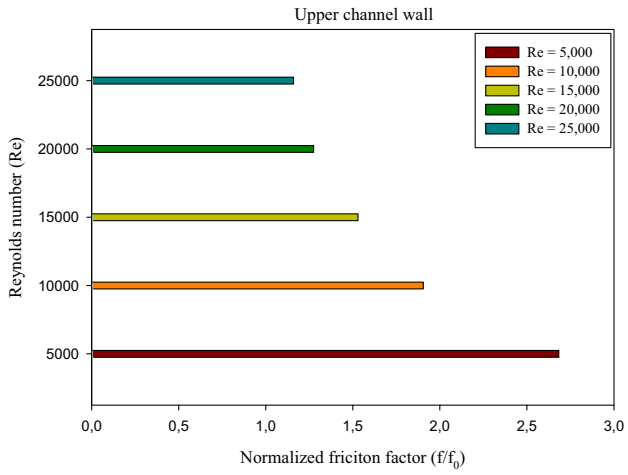

(b) Profiles of f/f_0

Fig. 15 Re effects on the local and average values of friction at the top channel wall

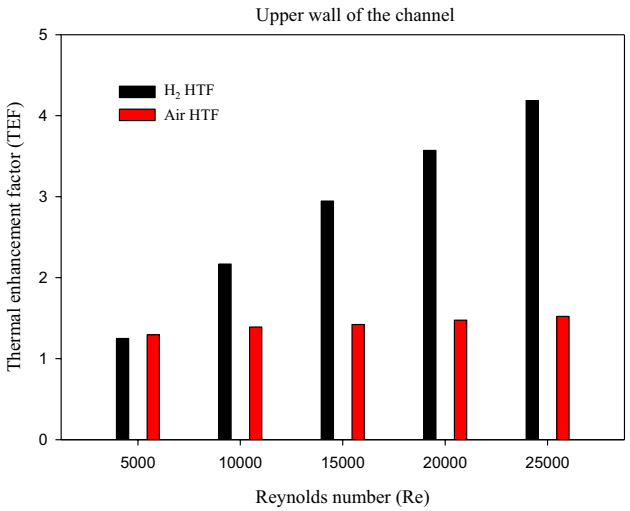

Fig. 16 Hydrothermal performance as a function of Re number for various HTFs

References

1. Ahmadi MH, Ghazvini M, Sadeghzadeh M, Alhuyi Nazari M, Kumar R, Naeimi A, Ming T (2018) Solar power technology for electricity generation: a critical review. Energy Sci Eng 6:340–361
2. Ahmadi MH, Ghazvini M, Sadeghzadeh M, Alhuyi Nazari M, Ghalandari M (2019) Utilization of hybrid nanofluids in solar energy applications: a review. Nano Struct Nano Objects 20:100386
3. Baharifard F, Parand K, Rashidi MM (2020) Novel solution for heat and mass transfer of a MHD micropolar fluid flow on a moving plate with suction and injection. Eng Comput. https://doi.org/10.1007/s00366-020-01026-7
4. Asadi A, Bakhtiyari AN, Alarifi IM (2020) Predictability evaluation of support vector regression methods for thermophysical properties, heat transfer performance, and pumping power estimation of MWCNT/ZnO-engine oil hybrid nanofluid. Eng Comput. https://doi.org/10.1007/s00366-020-01038-3
5. Abbasi A, Firouzi B, Sendur P (2019) On the application of Harris hawks optimization (HHO) algorithm to the design of microchannel heat sinks. Eng Comput. https://doi.org/10.1007/s00366-019-00892-0
6. Çelik İ (2019) Squeezing flow of nanofluids of Cu–water and kerosene between two parallel plates by Gegenbauer wavelet collocation method. Eng Comput. https://doi.org/10.1007/s00366-019-00821-1
7. Kudenatti RB, Jyothi B (2019) Computational and asymptotic methods for three-dimensional boundary-layer flow and heat transfer over a wedge. Eng Comput. https://doi.org/10.1007/s00366-019-00776-3
8. Alawee WH, Hassan JM, Mohammad WS (2016) Experimental and numerical study on the improvement of uniformity flow in a parallel flow channel. Eng Technol J Part (A) Eng 34(5):847–856
9. Hassan JM, Mohammed WS, Mohamed TA, Alawee WH (2014) CFD simulation for manifold with tapered longitudinal section. Int J Emerg Technol Adv Eng 4(2):28–35
10. Dhahad HA, Alawee WH, Hassan AK (2019) Experimental study of the effect of flow field design to PEM fuel cells performance. Renew Energy Focus 30:71–77
11. Alawee WH, Almolhem YA, Yusuf B, Mohammad TA, Dhahad HA (2020) Variation of coefficient of friction and friction head losses along a pipe with multiple outlets. Water 12(3):844
12. Hassan JM, Mohamed TA, Mohammed WS, Alawee WH (2014) Modeling the uniformity of manifold with various configurations. J Fluids. https://doi.org/10.1155/2014/325259
13. Dhahad HA, Al-Sumaily GF, Alawee WH, Thompson MC (2020) Aiding and opposing re-circulating mixed convection flows in a square vented enclosure. Therm Sci Eng Prog 19:100577
14. Alawee WH (2015) Improving the productivity of single effect double slope solar still by modification simple. J Eng 21(8):50–60
15. Hassan JM, Mohamed TA, Mohammed WS, Alawee WH (2015) Experimental and numerical study on the improvement of uniformity flow for three-lateral dividing manifold. Int J Eng Technol 12(1):29–37
16. Alawee WH, Hassan JM, Mohammad WS (2015) Effect of recirculation ratio on the uniformity flow in a high area ratio of outlets pipe at different entrance flow rates. J Eng 21(9):169–184
17. Ismael MA (2019) Forced convection in partially compliant channel with two alternated baffles. Int J Heat Mass Transf 142:118455
18. Alawee WH, Yusuf B, Mohammad TA, Dhahad HA (2019) Variation of flow along a multiple outlets pipe with various spacing and inflow water head based on physical model. J Eng Sci Technol 14:2399–2409
19. Liu J, Gao J, Gao T, Shi X (2013) Heat transfer characteristics in steam-cooled rectangular channels with two opposite rib-roughened walls. Appl Therm Eng 50:104–111
20. Ali M, Zeitoun O, Nuhait A (2011) Forced convection heat transfer over horizontal triangular cylinder in cross flow. Int J Therm Sci 50:106–114
21. Kumar A, Bhagoria JL, Sarviya RM (2009) Heat transfer and friction correlations for artificially roughened solar air heater duct with discrete W-shaped ribs. Energy Convers Manag 50:2017–2106
22. Karwa R, Maheshwari BK, Karwa N (2005) Experimental study of heat transfer enhancement in an asymmetrically heated rectangular duct with perforated baffles. Int Commun Heat Mass Transf 32:275–284
23. Kabeel AE, Hamed MH, Omara ZM, Kandeal AW (2018) Influence of fin height on the performance of a glazed and bladed entrance single-pass solar air heater. Sol Energy 162:410–419
24. Cao X, Du T, Liu Z, Zhai H, Duan Z (2019) Experimental and numerical investigation on heat transfer and fluid flow performance of sextant helical baffle heat exchangers. Int J Heat Mass Transf 142:118437
25. Saedodin S, Zamzamian SAH, Nimvari ME, Wongwises S, Jouybari HJ (2017) Performance evaluation of a flat-plate solar collector filled with porous metal foam: experimental and numerical analysis. Energy Convers Manag 153:278–287
26. Abchouyeh MA, Fard OS, Mohebbi R, Sheremet MA (2019) Enhancement of heat transfer of nanofluids in the presence of sinusoidal side obstacles between two parallel plates through the lattice Boltzmann method. Int J Mech Sci 156:159–169
27. Chompookham T, Thianpong C, Kwankaomeng S, Promvonge P (2010) Heat transfer augmentation in a wedge-ribbed channel using winglet vortex generators. Int Commun Heat Mass Transf 37:163169
28. Dutta P, Hossain A (2005) Internal cooling augmentation in rectangular channel using two inclined baffles. Int J Heat Fluid Flow 26:223–232

29. Kalaiarasi G, Velraj R, Swami MV (2016) Experimental energy and exergy analysis of a flat plate solar air heater with a new design of integrated sensible heat storage. Energy 111:609–619
30. Peng D, Zhang X, Dong H, Lv K (2010) Performance study of a novel solar air collector. Appl Therm Eng 30:2594–2601
31. Selimefendigil F, Oztop HF, Sheremet MA, Abu-Hamdeh N (2019) Forced convection of Fe_3O_4-water nanofluid in a bifurcating channel under the effect of variable magnetic field. Energies 12:666. https://doi.org/10.3390/en12040666
32. Chamkha AJ, Menni Y, Ameur H (2021) Thermal-aerodynamic performance measurement of air heat transfer fluid mechanics over S-shaped fins in shell-and-tube heat exchangers. J Appl Comput Mech. https://doi.org/10.22055/JACM.2020.32107.1970
33. Menni Y, Chamkha AJ, Ameur H, Ahmadi MH (2020) Hydrodynamic behavior in solar oil heat exchanger ducts fitted with staggered baffles and fins. J Appl Comput Mech. https://doi.org/10.22055/jacm.2020.32468.2021
34. Izadi M, Pour SH, Yasuri AK, Chamkha AJ (2019) Mixed convection of a nanofluid in a three-dimensional channel. J Therm Anal Calorim 136:2461–2475
35. Menni Y, Azzi A, Chamkha A (2019) The solar air channels: comparative analysis, introduction of arc-shaped fins to improve the thermal transfer. J Appl Comput Mech 5:616–626
36. Kamali R, Binesh AR (2008) The importance of rib shape effects on the local heat transfer and flow friction characteristics of square ducts with ribbed internal surfaces. Int Commun Heat Mass Transf 35:1032–1040
37. Umavathia JC, Sheremet MA (2016) Mixed convection flow of an electrically conducting fluid in a vertical channel using Robin boundary conditions with heat source/sink. Eur J Mech B Fluids 55:132–145
38. Nasiruddin Siddiqui MHK (2007) Heat transfer augmentation in a heat exchanger tube using a baffle. Int J Heat Fluid Flow 28:318–328
39. Wang F, Zhang J, Wang S (2012) Investigation on flow and heat transfer characteristics in rectangular channel with drop-shaped pin fins. Propuls Power Res 1:64–70
40. Eiamsa-ard S, Promvonge P (2008) Numerical study on heat transfer of turbulent channel flow over periodic grooves. Int Commun Heat Mass Transf 35:844–852
41. Ozceyhan V, Gunes S, Buyukalaca O, Altuntop N (2008) Heat transfer enhancement in a tube using circular cross sectional rings separated from wall. Appl Energy 85:988–1001
42. Promvonge P, Changcharoen W, Kwankaomeng S, Thianpong C (2011) Numerical heat transfer study of turbulent square-duct flow through inline V-shaped discrete ribs. Int Commun Heat Mass Transf 38:1392–1399
43. Sripattanapipat S, Promvonge P (2009) Numerical analysis of laminar heat transfer in a channel with diamond-shaped baffles. Int Commun Heat Mass Transf 36:32–38
44. Mohammadi Pirouz M, Farhadi M, Sedighi K, Nemati H, Fattahi E (2011) Lattice Boltzmann simulation of conjugate heat transfer in a rectangular channel with wall-mounted obstacles. Sci Iran 18:213–221
45. Mohammadi K, Sabzpooshani M (2014) Appraising the performance of a baffled solar air heater with external recycle. Energy Convers Manag 88:239–250
46. Mohammadi K, Sabzpooshani M (2013) Comprehensive performance evaluation and parametric studies of single pass solar air heater with fins and baffles attached over the absorber plate. Energy 57:741–750
47. Skullong S, Thianpong C, Jayranaiwachira N, Promvonge P (2016) Experimental and numerical heat transfer investigation in turbulent square-duct flow through oblique horseshoe baffles. Chem Eng Process Process Intensif 99:58–71
48. Priyam A, Chand P (2016) Thermal and thermohydraulic performance of wavy finned absorber solar air heater. Sol Energy 130:250–259
49. Hu J, Sun X, Xu J, Li Z (2013) Numerical analysis of mechanical ventilation solar air collector with internal baffles. Energy Build 62:230–238
50. Bayrak F, Oztop HF, Hepbasli A (2013) Energy and exergy analyses of porous baffles inserted solar air heaters for building applications. Energy Build 57:338–345
51. Youcef-Ali S, Desmons JY (2006) Numerical and experimental study of a solar equipped with offset rectangular plate fin absorber plate. Renew Energy 31:2063–2075
52. Dadvand A, Hosseini S, Aghebatandish S, Khoo BC (2019) Enhancement of heat and mass transfer in a microchannel via passive oscillation of a flexible vortex generator. Chem Eng Sci 207:556–580
53. Luo L, Wen F, Wang L, Sundén B, Wang S (2016) Thermal enhancement by using grooves and ribs combined with delta-winglet vortex generator in a solar receiver heat exchanger. Appl Energy 183:1317–1332
54. Muñoz-Cámara J, Crespí-Llorens D, Solano JP, Vicente PG (2020) Experimental analysis of flow pattern and heat transfer in circular-orifice baffled tubes. Int J Heat Mass Transf 147:118914
55. Mellal M, Benzeguir R, Sahel D, Ameur H (2017) Hydro-thermal shell-side performance evaluation of a shell and tube heat exchanger under different baffle arrangement and orientation. Int J Therm Sci 121:138–149
56. Miroshnichenko IV, Sheremet MA, Pop I, Ishak A (2017) Convective heat transfer of micropolar ßuid in a horizontal wavy channel under the local heating. Int J Mech Sci 128–129:541–549
57. Promvonge P, Sripattanapipat S, Tamna S, Kwankaomeng S, Thianpong C (2010) Numerical investigation of laminar heat transfer in a square channel with 45° inclined baffles. Int Commun Heat Mass Transf 37:170–177
58. Wen J, Yang H, Wang S, Xue Y, Tong X (2014) Experimental investigation on performance comparison for shell-and-tube heat exchangers with different baffles. Int J Heat Mass Transf 84:990–997
59. Yongsiri K, Eiamsa-Ard P, Wongcharee K, Eiamsa-Ard S (2014) Augmented heat transfer in a turbulent channel flow with inclined detached-ribs. Case Stud Therm Eng 3:1–10
60. Mokhtari M, Barzegar Gerdroodbary M, Yeganeh R, Fallah K (2017) Numerical study of mixed convection heat transfer of various fin arrangements in a horizontal channel. Eng Sci Technol Int J 20:1106–1114
61. Arjmandi H, Amiri P, Saffari Pour M (2020) Geometric optimization of a double pipe heat exchanger with combined vortex generator and twisted tape: a CFD and response surface methodology (RSM) study. Therm Sci Eng Prog 18:100514
62. Wang Y, Liu P, Shan F, Liu Z, Liu W (2019) Effect of longitudinal vortex generator on the heat transfer enhancement of a circular tube. Appl Therm Eng 148:1018–1028
63. Demartini LC, Vielmo HA, Möller SV (2004) Numeric and experimental analysis of the turbulent flow through a channel with baffle plates. J Braz Soc Mech Sci Eng 26:153–159
64. ANSYS Inc (2012) ANSYS Fluent 12.0, Theory Guide, ANSYS Inc., Canonburg, PA, USA
65. Yang YT, Hwang CZ (2003) Calculation of turbulent flow and heat transfer in a porous-baffled channel. Int J Heat Mass Transf 46:771–780
66. Dittus FW, Boelter LMK (1985) Heat transfer in automobile radiators of the tubular type. Int Commun Heat Mass Transf 12:3–22

67. Petukhov BS (1970) Heat transfer and friction in turbulent pipe flow with variable physical properties. Adv Heat Transf 6:503–564
68. Launder BE, Spalding DB (1974) The numerical computation of turbulent flows. Comput Methods Appl Mech Eng 3:269–289
69. Patankar SV (2018) Numerical heat transfer and fluid flow. CRC Press, Boca Raton. https://doi.org/10.1201/9781482234213